

## Potent, Highly Selective, and Orally Bioavailable Gem-Difluorinated Monocationic Inhibitors of Neuronal Nitric Oxide Synthase

Fengtian Xue,<sup>†,‡</sup> Huiying Li,<sup>‡</sup> Silvia L. Delker,<sup>‡</sup> Jianguo Fang,<sup>†</sup> Pavel Martásek,<sup>§,||</sup>  
Linda J. Roman,<sup>§</sup> Thomas L. Poulos,<sup>\*,‡</sup> and Richard B. Silverman<sup>\*,†</sup>

*Departments of Chemistry and Biochemistry, Molecular Biology, and Cell Biology, Center for Molecular Innovation and Drug Discovery, Chemistry of Life Processes Institute, Northwestern University, 2145 Sheridan Road, Evanston, Illinois 60208-3113, Departments of Molecular Biology and Biochemistry, Pharmaceutical Chemistry, and Chemistry, University of California, Irvine, California 92697-3900, Department of Biochemistry, University of Texas Health Science Center, San Antonio, Texas 78229, and Department of Pediatrics and Center for Applied Genomics, First School of Medicine, Charles University, Prague, Czech Republic*

Received July 12, 2010; E-mail: Agman@chem.northwestern.edu; poulos@uci.edu

**Abstract:** In our efforts to discover neuronal isoform selective nitric oxide synthase (NOS) inhibitors, we have developed a series of compounds containing a pyrrolidine ring with two stereogenic centers. The enantiomerically pure compounds, (S,S) versus (R,R), exhibited two different binding orientations, with (R,R) inhibitors showing much better potency and selectivity. To improve the bioavailability of these inhibitors, we have introduced a CF<sub>2</sub> moiety geminal to an amino group in the long tail of one of these inhibitors, which reduced its basicity, resulting in compounds with monocationic character under physiological pH conditions. Biological evaluations have led to a nNOS inhibitor with a K<sub>i</sub> of 36 nM and high selectivity for nNOS over eNOS (3800-fold) and iNOS (1400-fold). MM-PBSA calculations indicated that the low pK<sub>a</sub> NH is, at least, partially protonated when bound to the active site. A comparison of rat oral bioavailability of the difluorinated compound to the parent molecule shows 22% for the difluorinated compound versus essentially no oral bioavailability for the parent compound. This indicates that the goal of this research to make compounds with only one protonated nitrogen atom at physiological pH to allow for membrane permeability, but which can become protonated when bound to NOS, has been accomplished.

### Introduction

Since its first discovery as the endothelium-derived relaxing factor (EDRF) in 1987,<sup>1</sup> nitric oxide (NO) has emerged as an important biological messenger involved in a wide variety of physiological functions as well as pathophysiological states. In living organisms, NO is produced by nitric oxide synthase (NOS), a homodimeric flavohemoprotein, through the oxidation of L-arginine to L-citrulline with NADPH and O<sub>2</sub> as cosubstrates.<sup>2–4</sup>

To date, three distinct isoforms of mammalian NOS, namely, neuronal NOS (nNOS), inducible NOS (iNOS), and endothelial NOS (eNOS), have been identified with high homology (>55%).<sup>5</sup> nNOS catalyzes the oxidation of L-arginine in the central nervous system, generating NO as a critical neurotrans-

mitter.<sup>6,7</sup> Although normal activity of nNOS is important for neurotransmission, NO overproduction by nNOS has been shown to be associated with chronic neurodegenerative pathologies such as Parkinson's,<sup>8</sup> Alzheimer's,<sup>9</sup> and Huntington's diseases,<sup>10</sup> also with chronic headaches,<sup>11</sup> as well as neuronal damage in stroke.<sup>12</sup> iNOS, the isozyme of NOS that produces cytotoxic NO, is responsible for maintaining normal function of the immune system.<sup>13</sup> eNOS, on the other hand, regulates blood pressure. It has been shown experimentally that the reduced NO production by eNOS causes hypertension and atherosclerosis.<sup>14</sup> Therefore, selective inhibition of nNOS activ-

<sup>†</sup> Northwestern University.

<sup>‡</sup> Present address: Department of Chemistry, University of Louisiana at Lafayette, P.O. Box 44370, Lafayette, Louisiana 70504, USA.

<sup>§</sup> University of California.

<sup>§</sup> University of Texas Health Science Center.

<sup>||</sup> Charles University.

(1) Palmer, R. M. J.; Ferrige, A. G.; Moncada, S. *Nature* **1987**, *327*, 524.

(2) Marletta, M. A. *J. Biol. Chem.* **1993**, *268*, 12231.

(3) Marletta, M. A. *Cell* **1994**, *78*, 927.

(4) Griffith, O. W.; Stuehr, D. J. *Annu. Rev. Physiol.* **1995**, *57*, 707.

(5) Alderton, W. K.; Cooper, C. E.; Knowles, R. G. *Biochem. J.* **2001**, *357*, 593.

(6) Hall, A. V.; Antoniou, H.; Wang, Y.; Cheung, A. H.; Arbus, A. M.; Olson, S. L.; Lu, W. C.; Kau, C. L.; Marsden, P. A. *J. Biol. Chem.* **1994**, *269*, 33082.

(7) Wang, Y.; Newton, D. C.; Marsden, P. A. *Crit. Rev. Neurobiol.* **1999**, *13*, 21.

(8) Zhang, L.; Dawson, V. L.; Dawson, T. M. *Pharmacol. Ther.* **2006**, *109*, 33.

(9) Dorheim, M.-A.; Tracey, W. R.; Pollock, J. S.; Grammas, P. *Biochem. Biophys. Res. Commun.* **1994**, *205*, 659.

(10) Norris, P. J.; Waldvogel, H. J.; Faull, R. L. M.; Love, D. R.; Emson, P. C. *Neuroscience* **1996**, *72*, 1037.

(11) Ashina, M. *Exp. Opin. Pharmacother.* **2002**, *3*, 395.

(12) Sims, N. R.; Anderson, M. F. *Neurochem. Int.* **2002**, *40*, 511.

(13) Hobbs, A. J.; Higgs, A.; Moncada, S. *Annu. Rev. Pharmacol.* **1999**, *39*, 191.

(14) Dawson, V. L.; Dawson, T. M.; London, E. D.; Bredt, D. S.; Snyder, S. H. *Proc. Natl. Acad. Sci. U.S.A.* **1991**, *88*, 6368.

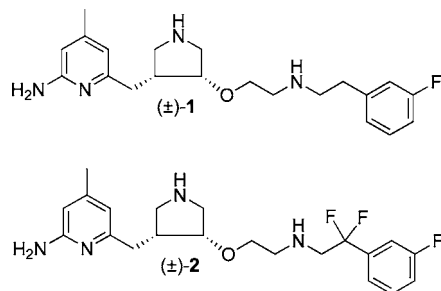


**Figure 1.** Chemical structures of **1** and **2**.

ity over its closely related isoforms, eNOS and iNOS, represents an exciting drug approach for the development of new therapeutic agents to treat neurodegenerative diseases.<sup>5,15,16</sup>

In our continuing efforts to develop nNOS selective inhibitors, we have discovered a pyrrolidine-based compound (**1**, Figure 1), which showed great potency ( $K_i = 15$  nM) and excellent selectivity for nNOS over eNOS (2100-fold) and iNOS (630-fold).<sup>17</sup> However, further application of this compound as a drug candidate for neurodegenerative diseases is limited by its poor bioavailability.<sup>18</sup> The two positive charges of **1** at physiological pH, derived from the two basic amino (NH) groups, dramatically impair the ability of **1** to penetrate the blood brain barrier (BBB) by passive diffusion.<sup>18</sup> In addition, the benzylic position of the *m*-fluorophenylethyl substituent is susceptible to metabolic oxidation.<sup>19</sup>

To circumvent these problems, different strategies have been employed to improve the bioavailability of inhibitors by limiting the number of basic functional groups in **1**.<sup>18,20,21</sup> For example, by incorporating an electron-withdrawing group adjacent to the amino group in the hydrophobic tail, a series of low  $pK_a$  inhibitors were synthesized with monocationic or pseudo-monocationic characters at physiological pH.<sup>20</sup> Evaluation of these inhibitors led to the discovery of inhibitor **2**, with two fluorines substituted at the benzylic position of the *m*-fluorophenylethyl tail of **1**. The racemic mixture of **2** indicated good potency ( $K_i = 80$  nM) and high selectivity for nNOS over both eNOS (1500-fold) and iNOS (650-fold). More importantly, it showed improved cell-membrane permeability compared to the parent compound **1**.<sup>20</sup> The CF<sub>2</sub> group is widely used in drug development because of its unique pharmacological properties.<sup>22</sup> For inhibitor **2**, the additional CF<sub>2</sub> group not only decreases the basicity of the adjacent amino group dramatically ( $pK_a \approx 5.5$ ), but also effectively blocks the potential metabolic oxidation at the benzylic position of the *m*-fluorophenyl ring.<sup>19</sup> We report here the structure-based design, synthesis, and biological evaluation of a series of enantiomerically pure inhibitors (**3a–f**)

derived from inhibitor **2**, in an attempt to further improve the pharmacodynamic and pharmacokinetic properties of these inhibitors.

## Results and Discussion

**Chemistry.** An improved synthesis of enantiomerically pure pyrrolidine core (**4a,b**) is shown in Scheme 1. First, racemic *trans*-alcohol **5** underwent a Mitsunobu reaction with (*S*)-(-)-camphanic acid as the nucleophile to produce two separable diastereomers (**6a** and **6b**) in excellent yields. Next, the ester in **6a** and **6b** was hydrolyzed in aqueous Na<sub>2</sub>CO<sub>3</sub> to generate **4a** and **4b** in high yields.

As shown in Scheme 2, single enantiomer **4a** or **4b** was treated with NaH, and the resulting anion was allowed to react with allyl bromide to generate **7a** and **7b** in excellent yields. Ozonolysis of **7a** and **7b** using Zn dust as the reducing reagent yielded **8a** and **8b** in good yields. Aldehydes **8a** and **8b** were subjected to reductive amination reactions with different ethanamines in the presence of NaHB(OAc)<sub>3</sub> to generate secondary amines, which were further protected by another Boc-protecting group to produce fully protected inhibitors **9a–d** in good yields. Next, the benzyl-protecting group was removed by catalytic hydrogenation using Pd(OH)<sub>2</sub> at 60 °C to provide **10a–d** in modest yields. Finally, the three Boc-protecting groups were removed at the same time in HCl to generate the final inhibitors (**3a–d**) in high yields.

The synthesis of inhibitor **3e** began with **9d** (Scheme 3). Catalytic hydrogenation of **9d** using Pd(OH)<sub>2</sub> at elevated temperature removed the benzyl-protecting group; when run for 48 h, the pyridinyl ring also was reduced to generate **10e** in modest yields. Then, the three Boc-protecting groups were removed in HCl to generate final inhibitor **3e** in high yields.

The synthesis of inhibitor **3f** is shown in Scheme 4. Reductive amination between aldehyde **8b** and 2,2-difluoro-2-(pyridin-2-yl)ethanamine generated a secondary amine, which was further protected by another Boc-protecting group to provide **9f** in good yields. Next, catalytic hydrogenation of **9f** removed the benzyl protecting group and also reduced the pyridinyl group adjacent to the CF<sub>2</sub> group to generate **10f** in modest yields. Finally, the three Boc-protecting groups were removed at the same time in HCl to generate inhibitor **3f** in high yields.

**Crystal Structures of nNOS with 3a–3f Bound.** Consistent with the binding preference of enantiomerically pure parental compound **1**,<sup>23</sup> the binding mode of these difluorinated derivatives is also dependent on the configuration around the two chiral centers, the 3' and 4' positions, of the pyrrolidine ring. While (*S,S*) inhibitor **3a** was found to bind with its aminopyridine moiety hydrogen bonded to the side chain of Glu592 in nNOS (Figure 2A), (*R,R*) inhibitor **3b** adopted a 180° flipped binding mode with its aminopyridine making bifurcated hydrogen bonds with the heme propionate of pyrrole ring D (Figure 2B). To make room for these new hydrogen bonds, the Tyr706 side chain rotates away and  $\pi$ -stacks against the aminopyridine ring of the inhibitor. The pyrrolidine nitrogen in **3b** also makes favorable hydrogen bonds with propionate A as well as the O4 atom of H<sub>4</sub>B. In comparison, the pyrrolidine nitrogen in **3a** is only loosely hydrogen bonded to Glu592. The long, flexible linker extending from the pyrrolidine allows the fluorophenyl group in **3b** to reach the vicinity of Glu592 and to  $\pi$ -stack with the heme. The amino group vicinal to the CF<sub>2</sub> moiety points

(15) Southan, G. J.; Szabo, C. *Biochem. Pharmacol.* **1996**, *51*, 383.

(16) Babu, B. R.; Griffith, O. W. *Curr. Opin. Chem. Biol.* **1998**, *2*, 491.

(17) Ji, H.; Li, H.; Martásek, P.; Roman, L. J.; Poulos, T. L.; Silverman, R. B. *J. Med. Chem.* **2009**, *52* (3), 779.

(18) Lawton, G. R.; Ranaivo, H. R.; Wing, L. K.; Ji, H.; Xue, F.; Martásek, P.; Roman, L. J.; Watterson, D. M.; Silverman, R. B. *Bioorg. Med. Chem.* **2009**, *17*, 2371.

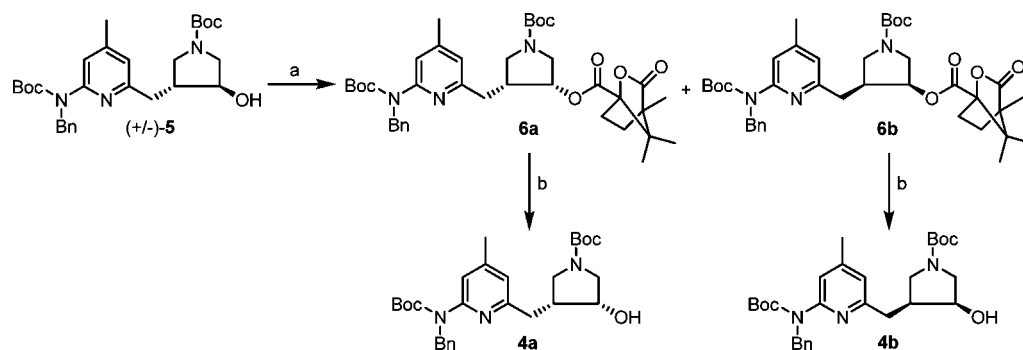
(19) Silverman, R. B. *The Organic Chemistry of Drug Design and Drug Action*, 2nd ed.; Elsevier: Boston, MA, 2004.

(20) Xue, F.; Fang, J.; Lewis, W. W.; Martásek, P.; Roman, L. J.; Silverman, R. B. *Bioorg. Med. Chem. Lett.* **2010**, *20*, 554.

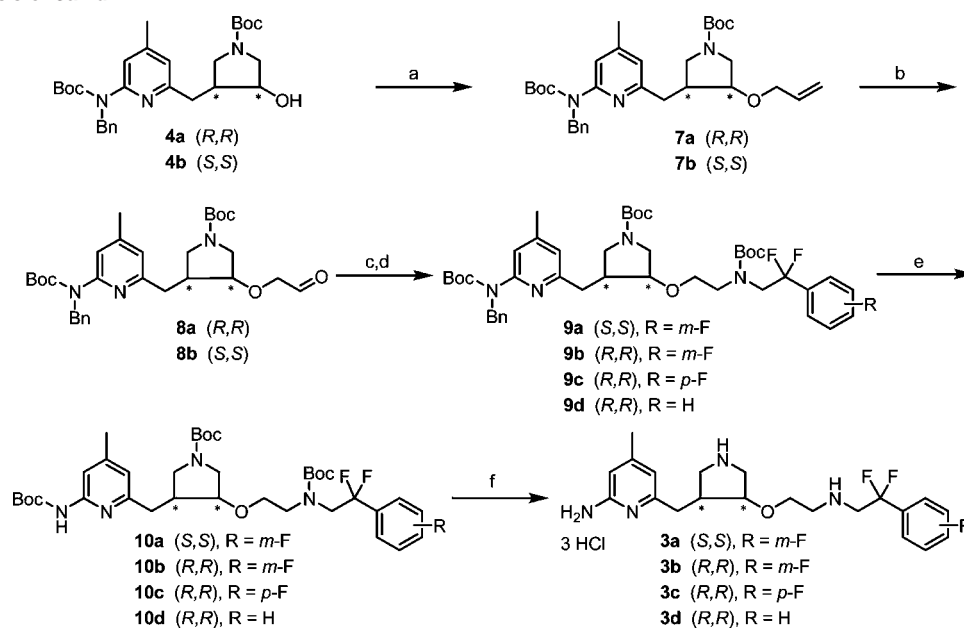
(21) Xue, F.; Huang, J.; Ji, H.; Fang, J.; Li, H.; Martásek, P.; Roman, L. J.; Poulos, T. P.; Silverman, R. B. *Bioorg. Med. Chem.* **2010**, *18*, 6526.

(22) Smart, B. E. *J. Fluorine Chem.* **2001**, *109*, 3.

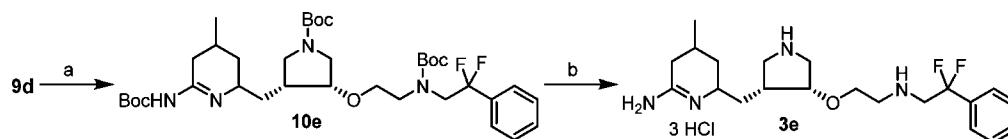
(23) Delker, D. L.; Ji, H.; Li, H.; Jamal, J.; Fang, J.; Xue, X.; Silverman, R. B.; Poulos, T. L. *J. Am. Chem. Soc.* **2010**, *132*, 5437.

Scheme 1. Synthesis of 4a,b<sup>a</sup>

<sup>a</sup> Reagents and conditions: (a) (*S*)-(-)-camphanic acid, PPh<sub>3</sub>, DIAD, rt, 16 h, 95%; (d) Na<sub>2</sub>CO<sub>3</sub>, rt, 4 h, 95%.

Scheme 2. Synthesis of 3a–d<sup>a</sup>

<sup>a</sup> Reagents and conditions: (a) (i) NaH, (ii) allyl bromide, rt, 1 h, 96%; (b) O<sub>3</sub>, –78 °C, (ii) Zn, –78 °C to rt, 2 h, 81%; (c) (i) ethanamines, THF, rt, 5 min, (ii) NaHB(OAc)<sub>3</sub>, rt, 3 h; (d) (Boc)<sub>2</sub>O, Et<sub>3</sub>N, MeOH, rt, 3 h, 48–60% for two steps; (e) Pd(OH)<sub>2</sub>/C, H<sub>2</sub>, EtOH, 60 °C, 30 h, 45–60%; (f) 6 N HCl/MeOH (2:1), rt, 16 h, 95–100%.

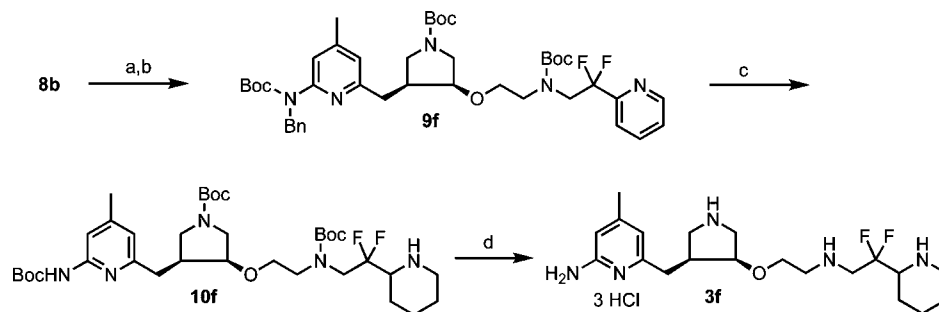
Scheme 3. Synthesis of 3e<sup>a</sup>

<sup>a</sup> Reagents and conditions: (a) Pd(OH)<sub>2</sub>/C, H<sub>2</sub>, EtOH, 60 °C, 48 h, 55%; (d) 6 N HCl/MeOH (2:1), rt, 16 h, 96%.

toward the Glu592 side chain, resulting in an alternate conformation of the carboxylate enabling a hydrogen bond to form between the amino nitrogen and the carboxylate oxygen (Figure 2B). This alternate conformation of Glu592 was not observed in the structure of nNOS bound with 3a because the tight bifurcated hydrogen bonds from the inhibitor aminopyridine to the carboxylate of Glu592 made an excellent match to the original conformation of the Glu side chain. The fit of the fluorophenyl group in 3b near Glu592 is not ideal, and to avoid close van der Waals contacts with the inhibitor, Glu592 adopts the alternate conformation. In addition, the fluorophenyl tail of 3b is disordered, as indicated by the weak electron density for this group. When only one conformation of the tail was modeled with the two fluorine atoms pointing away from the heme plane,

strong negative difference density clustered around the fluorine atoms. Also, the electron density of the fluorophenyl ring could not be accounted for with only one ring orientation. The tail portion of 3b was, therefore, modeled with two different conformations (0.6 and 0.4 occupancy) as shown in Figure 2B. There also is a partially occupied site for a water molecule bridging between the heme propionate and the amino group in the tail portion of 3b in the minor conformation. In contrast, the fluorophenyl ring in 3a fits into a pocket formed by Met336, Leu337, and Tyr706 (Figure 2A), but the density for 3a is clear only up to the position of the two fluorine atoms, thus, precluding determination of the fluorophenyl ring orientation.

Inhibitor 3c has its fluorine position in the phenyl ring changed from *meta* in 3b to *para* in 3c. Because the C–F bond

Scheme 4. Synthesis of **3f**<sup>a</sup>

<sup>a</sup> Reagents and conditions: (a) (i) 2,2-difluoro-2-(pyridin-2-yl)ethanamine, THF, rt, 5 min; (ii) NaBH(OAc)<sub>3</sub>, rt, 3 h; (b) (Boc)<sub>2</sub>O, Et<sub>3</sub>N, MeOH, rt, 3 h, 55% for two steps; (c) Pd(OH)<sub>2</sub>/C, H<sub>2</sub>, EtOH, 60 °C, 30 h, 60%; (d) 2 N HCl/MeOH (1:1), rt, 16 h, 100%.

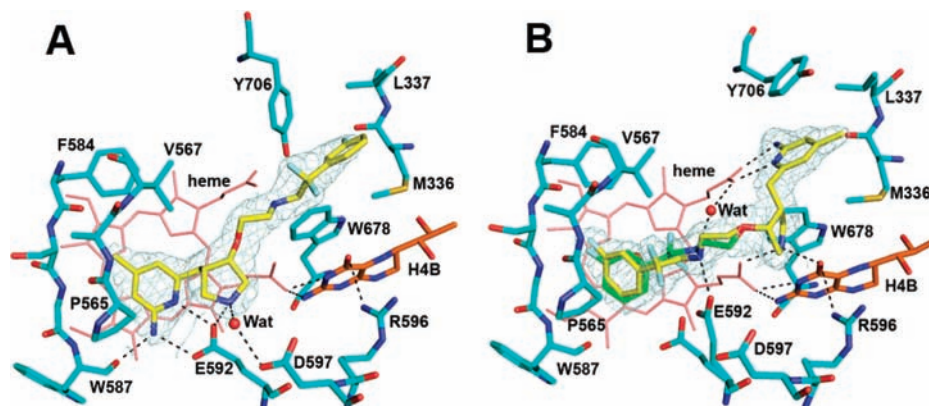


**Figure 2.** The nNOS active site with inhibitor **3a** (A) or **3b** (B) bound. The sigmaA weighted  $2F_o - F_c$  density for inhibitor is also shown at contour level of  $1\sigma$ . Hydrogen bonds are depicted with dashed lines. The atomic color schemes are: N, blue; O, red; S, yellow; F, light cyan. Alternate conformations for **3b** (yellow and green) and E592 were observed. Figures 2–4 were prepared with PyMol (<http://www.pymol.org>).

is 1.34 Å, **3c** is at least 1.3 Å longer than **3b**. As a result, the *para*-F in **3c** makes a H-bond directly to the protein backbone amide (Gly586), while the *meta*-F of **3b** makes only a weak van der Waals contact with the protein (Figure 3A). Because of the tighter contact of **3c**, the CF<sub>2</sub> moiety is forced into a downward conformation. The major conformation in **3b**, however, has the CF<sub>2</sub> moiety pointing upward. The downward conformation causes clashes between the CF<sub>2</sub> and heme propionate A, so the upward CF<sub>2</sub> conformation of **3b** represents a more relaxed fit in the active site, leading to higher potency.

Inhibitor **3d** is a derivative of **3b** and differs only by the absence of the fluorine on the phenyl ring. Its binding mode to nNOS is, therefore, almost identical to that of **3b** (Figure 3B). Without the *meta*-fluorine, the phenyl ring makes a looser contact with the hydrophobic pocket defined by Pro565, Val567, and Phe584. The phenyl tail portion in **3d** exhibits two alternate conformations similar to what is observed for **3b**.

Inhibitor **3e** has its aminopyridine ring partially reduced from that in **3d**, which has a negligible impact on the binding mode of the inhibitor compared to **3d** (Figure 3C). The amino and the ring nitrogens remain planar and are still tightly hydrogen bonded to the heme propionate of pyrrole D, and the pyrrolidine nitrogen is hydrogen bonded to propionate A and H<sub>4</sub>B. As in **3b** and **3d**, the phenyl tail in **3e** shows two conformations above the heme plane, and the Glu592 side chain also has two corresponding conformations.

Another (*S,S*) inhibitor, **3f**, is similar to **3a** except the fluorophenyl tail has been replaced by a piperidine ring. The binding of **3f** is similar to **3a** with its aminopyridine hydrogen bonded to the Glu592 side chain while the piperidine ring fits

into the pocket of Met336, Leu337, and Tyr706 (Figure 3D). The density for the tail portion is good only up to the CF<sub>2</sub> moiety with the piperidine partially disordered. Therefore, the orientation of the ring (position of nitrogen) is not well-defined.

**Crystal Structures of eNOS with 3b and 3f Bound.** The eNOS structure bound with (*R,R*) inhibitor **3b** (Figure 4A) shows that it has adopted a ‘flipped’ binding mode, the same orientation as in nNOS. The Tyr477 side chain rotates farther out than in nNOS and, therefore, does not experience optimized  $\pi$ -stacking interactions with the aminopyridine of the inhibitor, as was observed in nNOS. Similar to what was seen in nNOS, the aminopyridine in **3b** makes bifurcated hydrogen bonds with the heme propionate of pyrrole ring D, while the pyrrolidine nitrogen makes favorable hydrogen bonds with propionate A as well as the O4 atom of H<sub>4</sub>B (Figure 4A). A hydrogen bond between the inhibitor amino group with alternate conformations for Glu363 also is observed. With the available density at the limited resolution, only one conformation of the fluorophenyl tail portion can be modeled.

The binding of the (*S,S*) inhibitor **3f** in eNOS is similar to that in nNOS, with its aminopyridine hydrogen bonded to the Glu363 side chain (Figure 4B) in the normal binding mode. The pyrrolidine nitrogen also hydrogen bonds with the conserved glutamate residue, but the density for the tail portion is good only up to the CF<sub>2</sub> moiety with the piperidine partially disordered. Therefore, the orientation of the ring (position of nitrogen) and the exact configuration of the puckered ring are not clear.

**Inhibitory Assays and Structure-Based Evaluation.** Inhibitors **3a–f** were evaluated for *in vitro* inhibition activities against

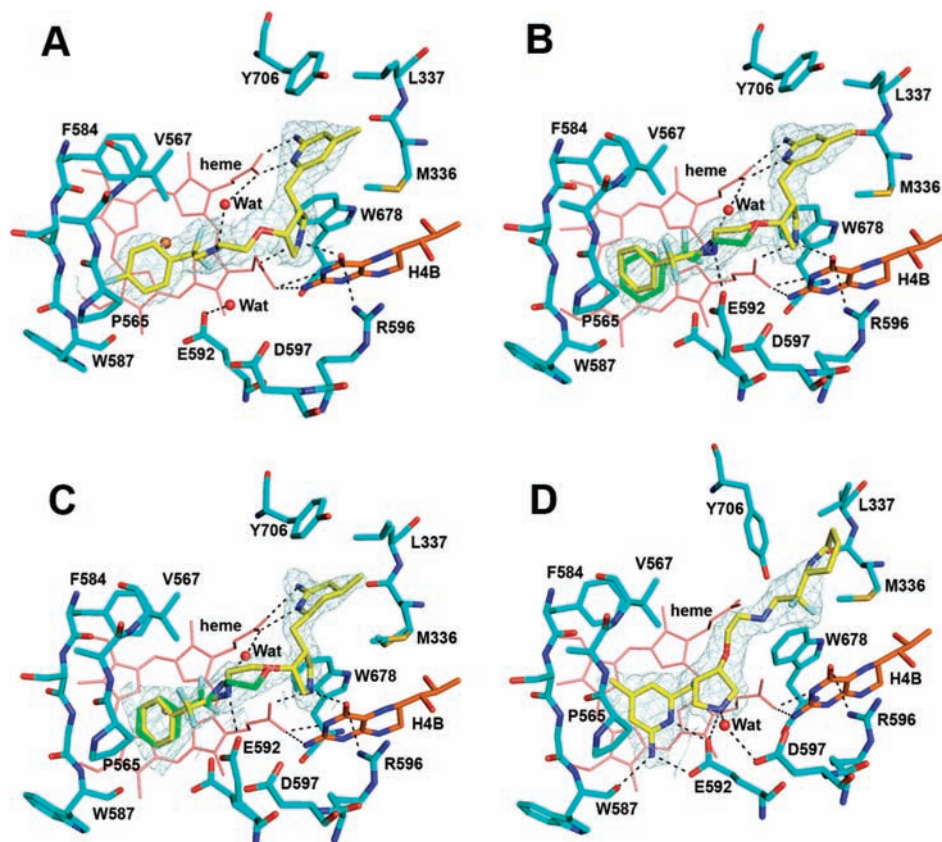


**Figure 3.** The nNOS active site with **3c** (A), **3d** (B), **3e** (C), or **3f** (D) bound. Around each inhibitor is the sigmaA weighted  $2F_o - F_c$  density contoured at  $1\sigma$ . Major hydrogen bonds are depicted with dashed lines. The same atomic color schemes as in Figure 1 are used. Note the alternate conformations for E592 occur when the inhibitor shows multiple conformations in the nNOS-**3d** or nNOS-**3e** structure.

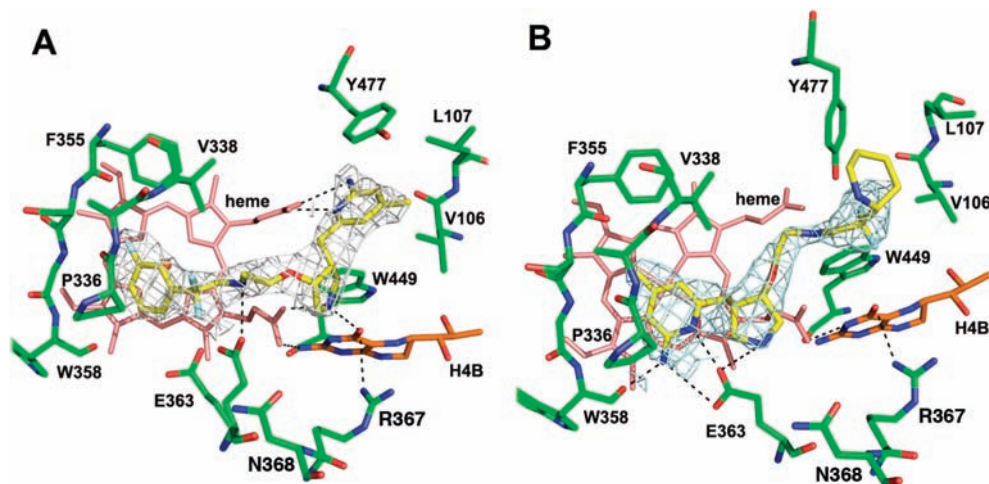


**Figure 4.** The eNOS active site with **3b** (A) and **3f** (B) bound. Around each inhibitor is the sigmaA weighted  $2F_o - F_c$  density contoured at  $1\sigma$ . Major hydrogen bonds are depicted with dashed lines. The same atomic color schemes as that in Figure 2 are used. As observed with nNOS, alternate conformations for Glu363 occur in the eNOS-**3b** structure.

three isozymes of NOSs including rat nNOS, bovine eNOS, and murine iNOS,<sup>24</sup> as summarized in Table 1. Compared to racemic lead compound **2**, (*S,S*) enantiomer **3a** is a weak inhibitor of nNOS with a  $K_i$  value of 390 nM, which is 5-fold less potent than **2**. In addition, the selectivity of this inhibitor for nNOS over eNOS and iNOS also decreases by 5-fold and 2-fold, respectively. The (*R,R*) enantiomer (**3b**), however, shows excellent potency for nNOS ( $K_i = 36$  nM) and remarkable

selectivity over eNOS (3800-fold) and iNOS (1400-fold). These results indicate that the chirality around the *cis*-chiral pyrrolidine core plays a key role in determining the potency and selectivity of inhibitors, as we have observed for another series of *trans*- or *cis*-chiral pyrrolidine inhibitors.<sup>23</sup> The potency and selectivity shown with racemic compound **2** can be attributed mainly to (*R,R*)-component **3b**. We now know that a large difference in binding affinity to nNOS between **3a** and **3b** originates from two different binding modes.<sup>23</sup> The flipped binding mode of **3b** relative to **3a** allows both the aminopyridine and pyrrolidine

(24) Hevel, J. M.; Marletta, M. A. *Methods Enzymol.* **1994**, *233*, 250.

**Table 1.**  $K_i^a$  Values of Inhibitors for Rat nNOS, Bovine eNOS, and Murine iNOS

compound	nNOS ( $\mu\text{M}$ )	eNOS ( $\mu\text{M}$ )	iNOS ( $\mu\text{M}$ )	selectivity <sup>b</sup>	
				n/e	n/i
<b>2</b>	0.080	120	52	1500	650
<b>3a</b>	0.390	110	130	280	330
<b>3b</b>	0.036	140	51	3800	1400
<b>3c</b>	0.160	31	190	190	1200
<b>3d</b>	0.085	130	85	1500	1000
<b>3e</b>	0.170	130	26	770	150
<b>3f</b>	2.70	64	450	24	170

<sup>a</sup> The  $K_i$  values were calculated based on the directly measured  $\text{IC}_{50}$  values, which represent at least duplicate measurements with standard deviations of  $\pm 10\%$ . <sup>b</sup> The ratio of  $K_i$  (eNOS or iNOS) to  $K_i$  (nNOS).

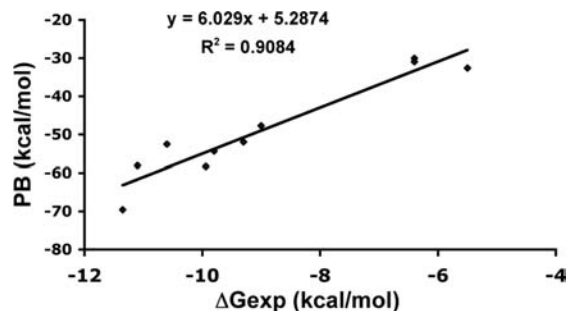
nitrogen atoms to make extensive hydrogen bonds with the heme and  $\text{H}_4\text{B}$  (Figure 2B). In addition, as we have argued elsewhere,<sup>23</sup> the conformation of **3a** when bound to NOS places the pyrrolidine nitrogen atom very close to the aminopyridine, and because of electrostatic repulsion, this aminopyridine is only partially protonated. However, in the **3b** flipped orientation, the aminopyridine is farther from the pyrrolidine nitrogen atom and remains fully protonated. Thus, the **3b** conformation provides greater electrostatic stabilization than the **3a** conformation, which accounts for the 10-fold lower  $K_i$  for **3b** than **3a**.

As a *p*-fluorophenyl derivative of **3b**, inhibitor **3c** shows a significant drop in potency for nNOS ( $K_i = 160$  nM), which is 4.5-fold less potent than **3b**. More interestingly, **3c** loses 20-fold of selectivity over eNOS observed with **3b** by moving one single F atom from the *m*-position to the *p*-position of the phenyl tail. The new fluorine position leads to a 'difluoromethylene-down' binding mode of the inhibitor's phenyl tail. As a result, the hydrogen bond between the Glu592 side chain and the amino nitrogen in the tail seen in **3b** has been eliminated, which may explain the weaker potency and selectivity of **3c**.

Inhibitor **3d**, with the F atom removed from the phenyl tail, has restored good potency for nNOS ( $K_i = 85$  nM) and high isozyme-selectivity (1500-fold over eNOS and 1000-fold over iNOS). This is because **3d** has retained the binding mode of **3b**. The only difference is that without a fluorine atom on the phenyl ring the van der Waals contacts to the protein (Pro565, Val567, and Phe584) are less optimal compared to that for **3b**. This results in a bit less potency and selectivity for **3d** than **3b**.

The amidino inhibitor **3e**, with the aromatic system of the aminopyridine fragment partially reduced, exhibits only a 2-fold drop in potency against nNOS compared to **3d**. Although  $\pi$ - $\pi$  stacking of **3e** with Tyr706 should be greatly diminished relative to that with **3d**, the increased basicity of the amidine of **3e** over the aminopyridine of **3d** may compensate by producing a tighter electrostatic interaction with the heme propionate, resulting in only a factor of 2 difference for the  $K_i$  values of the these inhibitors. The removal of the aromatic system of the aminopyridine ring from inhibitor **3d** allows **3e** to bind more than 3-fold better to iNOS, thus, exhibiting a much lower selectivity.

Finally, inhibitor **3f**, with an (*S,S*) configuration of the pyrrolidine core and a piperidiny tail, showed poor inhibition activity and isozyme-selectivity. Both **3a** and **3f** have similar binding orientations and rather poor potency among the inhibitors reported in this work. This result emphasizes again that the chirality of the pyrrolidine core is the key to higher inhibitory activity with (*R,R*) inhibitors. In addition, a less polar aromatic ring such as the fluorophenyl group in **3a** seems to fit better into the pocket surrounded by Met336, Leu337, and Tyr706 in

**Figure 5.** Plot of the computed free energy (PB) vs experimental free energy ( $\Delta G_{\text{exp}}$ ) obtained from  $K_i$  values.

nNOS than does the polar piperidiny ring in **3f**, and the  $\pi$ -stacking with the heme is lost in the case of **3f**. However, both **3a** and **3f** bind to eNOS with similar potency, possibly because of the smaller Val106 side chain in the pocket in eNOS compared to Met336 in nNOS.

The isoform selection shown for this series of inhibitors in Table 1 is not that straightforward to interpret based only on the structures presented here. For any one particular inhibitor among those reported in Table 1, the binding mode in eNOS is no different from that seen in nNOS. Similar to what we have discussed for another series of chiral pyrrolidine containing inhibitors,<sup>23</sup> one of the potential reasons for the isoform selectivity shown by **3b** is the difference in  $\pi$ -stacking interaction between the aminopyridine and Tyr706 in nNOS (or Tyr 477 in eNOS). We have consistently observed tighter interactions between this Tyr and the aminopyridine with nNOS complexed with inhibitors that adopt the **3b** flipped orientation.<sup>23</sup>

**Calculations To Determine the Protonation State of Bound Inhibitors.** The principal aim of this research was to lower the  $\text{p}K_a$  of one of the NH groups in the inhibitors, so that, at physiological pH, there would be effectively only one positive charge on the molecules, which should be acceptable for CNS penetration.<sup>25</sup> However, on the basis of past results, two positive charges are required for potency and isozyme selectivity. The aim was to find the appropriate  $\text{p}K_a$  so that, once bound to NOS, the low  $\text{p}K_a$  NH would become protonated and could undergo the appropriate electrostatic interaction with a carboxylate.

In our initial work on flipped inhibitors,<sup>23</sup> we employed the Molecular Mechanics Poisson–Boltzmann/Surface Area (MM-PBSA)<sup>26</sup> computational method to calculate the free energy of binding of a series of aminopyridine inhibitors to nNOS and eNOS. We employed the empirical equation derived from Figure 5,  $\Delta G_{\text{calc}} = (\text{PB} - 5.2874)/6.029$ , to obtain computed free energies. In our earlier work<sup>23</sup> we found that the best fits with  $\Delta G_{\text{exp}}$  resulted when the orientation of the inhibitor with the aminopyridine stacked over the heme (normal orientation) was assumed to be 50% protonated, while in the flipped orientation in which the aminopyridine interacts with the heme propionate, a +1 charge was assigned to the aminopyridine. The way partial charges were handled was to carry out the MM-PBSA calculations with a 0 or +1 charge and average the results. We carried out the same types of calculations with the difluorinated inhibitors used in this study, but the goal was to probe the state of protonation of the NH group whose  $\text{p}K_a$  has been lowered to  $\approx 5.5$  as a result of the fluorine atoms. The results of these calculations are shown in Table 2. With inhibitor **3b**, additional

(25) Kerns, E. H.; Di, L. *Drug-like Properties: Concepts, Structure Design and Methods*; Academic Press: Amsterdam, 2008; p 130.

(26) Massova, I.; Kollman, P. A. *J. Am. Chem. Soc.* **1999**, 8133.

**Table 2.** Calculated Free Energies for Three Inhibitors Used in This Study Assuming Different Charges<sup>a</sup>

inhibitor	charge on pyrrolidine	charge on NH	charge on amino pyridine	PB	$\Delta G_{\text{calc}}$	$\Delta G_{\text{exp}}$	$\Delta\Delta G$
<b>3a</b>	1	1	1	-77.3	-13.70	-8.8	4.90
<b>3a</b>	1	1	0	-47.66	-8.78	-8.8	0.018
<b>3a</b>	1	0	0	-18.75	-3.99	-8.8	4.81
	<b>average</b>				<b>-8.82</b>	<b>-8.8</b>	<b>0.022</b>
<b>3c</b>	1	0	1	-24.02	-4.86	-7.92	3.06
<b>3c</b>	1	1	1	-55.9	-10.15	-7.92	2.23
	<b>average</b>				<b>-7.50</b>	<b>-7.92</b>	<b>0.42</b>
<b>3b A</b>	1	1	1	-66.03	-11.83	-10.2	1.63
<b>3b B</b>	1	1	1	-82.7	-14.59	-10.2	4.39
<b>3b A</b>	1	0	1	-45.02	-8.34	-10.2	1.86
<b>3b B</b>	1	0	1	-36.25	-6.89	-10.2	3.31
	<b>average</b>				<b>-10.41</b>	<b>-10.2</b>	<b>0.21</b>

<sup>a</sup> For **3b**, two different conformations of the inhibitor were observed in the crystal structure referred to here as conformations A and B.

calculations were carried out because we observed two orientations in the nNOS active site. The best fit to  $\Delta G_{\text{exp}}$  results from assigning a full +1 charge to the aminopyridine in the “flipped” orientation and a +0.5 charge in the “normal” orientation and a +0.5 charge for the NH group in all the inhibitors independent of orientation. Our strategy for lowering the  $pK_a$  of the NH group was to decrease the total charge of the inhibitors in solution for better bioavailability but with the hope that they would become at least partially protonated once bound in the active site, where the nearby heme propionates and Glu592 might promote protonation. The calculations support this scenario and indicate that the NH group is partially protonated. This is reasonable because the NH group in these inhibitors, no matter which binding orientation, always H-bonds with one carboxylate and is within 4 Å from another carboxylate (either the Glu592 side chain or the heme propionate).

**Pharmacokinetic Data for 3b and (R,R)-1.** The goal for insertion of two *gem*-fluorines into **1** was to lower the  $pK_a$  of one of the two basic nitrogen atoms to enhance metabolic stability and oral bioavailability but allow for potential reprotonation of that nitrogen atom once in the active site of nNOS. Pharmacokinetic properties of compound **3b** (the *(R,R)* isomer of the *gem*-difluorinated analogue corresponding to *(R,R)*-**1**) were compared to those of *(R,R)*-**1** to determine the effect of the difluorine substitution on pharmacokinetics. The *in vivo* compound half-life ( $t_{1/2}$ ) for *iv* dosing at 1 mg/kg in rats (average of 3 rats) was 0.33 h for *(R,R)*-**1** and 7.5 h for **3b**; the  $t_{1/2}$  for oral dosing at 5 mg/kg was too low to measure for *(R,R)*-**1** and 3.7 h for **3b**; oral bioavailability for *(R,R)*-**1** was essentially 0 and 22.2% for **3b**. It is apparent that the addition of the two fluorines has a remarkable effect on *in vivo* stability and oral bioavailability.

In summary, we have designed and synthesized a new series of selective nNOS inhibitors (**3a–f**) with monocationic character and, therefore, potentially possessing better bioavailability. Biological evaluation of these new inhibitors based on crystal structures led to the discovery of inhibitor **3b**, which not only retains most of the inhibitory activity of lead compound **1**, but also shows remarkable selectivity for nNOS over both eNOS and iNOS. MM-PBSA calculations demonstrate that despite the  $pK_a$  of one of the nitrogen atoms in **3b** being 5.5, when bound to the active site, it becomes partially protonated for good binding. Whereas the *in vivo* half-life ( $t_{1/2}$ ) and oral bioavailability in rats for the parent compound [*(R,R)*-**1**] are nil, when the two fluorines are added (**3b**), the  $t_{1/2}$  rises to 10 h and oral bioavailability increases to 22%. This work represents a significant step forward toward the goal of developing drugs

with therapeutic potential in the treatment of diseases caused by unregulated NO generation from nNOS.

## Experimental Section

**1. General Methods.** All experiments were conducted under anhydrous conditions in an atmosphere of argon, using flame-dried apparatus and employing standard techniques in handling air-sensitive materials. All solvents were distilled and stored under an argon or nitrogen atmosphere before use. All reagents were used as received. Aqueous solutions of sodium bicarbonate, sodium chloride (brine), and ammonium chloride were saturated. Analytical thin layer chromatography was visualized by ultraviolet, ninhydrin, or phosphomolybdic acid (PMA). Flash column chromatography was carried out under a positive pressure of nitrogen. <sup>1</sup>H NMR spectra were recorded on 500 MHz spectrometers. Data are presented as follows: chemical shift (in ppm on the  $\delta$  scale relative to  $\delta = 0.00$  ppm for the protons in TMS), integration, multiplicity (s = singlet, d = doublet, t = triplet, q = quartet, m = multiplet, br = broad), coupling constant (*J*/Hz). Coupling constants were taken directly from the spectra and are uncorrected. <sup>13</sup>C NMR spectra were recorded at 125 MHz, and all chemical shift values are reported in ppm on the  $\delta$  scale, with an internal reference of  $\delta$  77.0 or 49.0 for CDCl<sub>3</sub> or MeOD, respectively. High-resolution mass spectra were measured on liquid chromatography/time-of-flight mass spectrometry (LC-TOF).

### 2. Preparation and Characterization of New Compounds.

**2.1. General Method A: Reductive Amination.** To a solution of aldehyde **8a** or **8b** (0.1 mmol) in THF (3 mL) was added the ethanamine (0.2 mmol), followed by NaHB(OAc)<sub>3</sub> (0.12 mmol). The mixture was stirred at room temperature for an additional 3 h and then concentrated. The crude product was purified by flash column chromatography (EtOAc/hexanes, 2:1–4:1) to yield the corresponding secondary amines as colorless oils, which were used without further purification.

**2.2. General Method B: Boc-Protection.** To a solution of the secondary amine (0.5 mmol) in MeOH (10 mL) was added (Boc)<sub>2</sub>O (164 mg, 0.75 mmol) and TEA (140  $\mu$ L, 1.0 mmol). The reaction mixture was allowed to stir at room temperature for 30 min. The solvent was removed by rotary evaporation, and the resulting material was purified by flash column chromatography (EtOAc/hexanes, 1:4–1:2) to yield **9a–f** as colorless oils.

**2.3. General Method C: Catalytic Hydrogenation.** To a solution of **9a–f** (0.2 mmol) in EtOH (20 mL) was added Pd(OH)<sub>2</sub>/C (100 mg). The reaction vessel was charged with H<sub>2</sub>, heated at 60 °C for 24–48 h, then cooled to room temperature. The catalyst was removed by filtration, and the resulting solution was concentrated by rotary evaporation. The crude material was purified by flash column chromatography (EtOAc/hexanes, 1:4–1:2) to yield **10a–f** as white foamy solids.

**2.4. General Method D: Boc-Deprotection.** To a solution of **10a–f** (50  $\mu$ mol) in MeOH (0.5 mL) was added 6 N HCl (1.0 mL). The reaction mixture was allowed to stand at room temperature

for 12 h. The solvent was removed by rotary evaporation. The crude product was recrystallized with cold diethyl ether to provide **3a–f** as pale yellow solids.

**(9a).** **9a** was synthesized by general methods A and B using aldehyde **8b** as the starting material (60%):  $^1\text{H}$  NMR (500 MHz,  $\text{CDCl}_3$ )  $\delta$  1.35–1.55 (m, 27H), 2.20–2.40 (s, 3H), 2.50–2.80 (m, 2H), 2.80–2.95 (m, 1H), 3.00–3.21 (m, 2H), 3.30–3.79 (m, 6H), 3.80–4.00 (m, 2H), 5.10–5.25 (s, 2H), 6.60–6.70 (br s, 1H), 7.00–7.30 (m, 8H), 7.31–7.60 (m, 2H);  $^{13}\text{C}$  NMR (125 MHz,  $\text{CDCl}_3$ )  $\delta$  14.4, 21.2, 21.3, 27.8, 28.1, 28.4, 28.5, 28.7, 29.9, 34.8, 42.3, 42.9, 47.5, 47.7, 49.0, 49.4, 50.1, 50.4, 50.9, 60.6, 67.9, 76.9, 78.9, 79.3, 79.7, 79.8, 80.6, 81.4, 113.0, 113.1, 117.2, 117.5, 120.1, 121.4, 126.7, 126.8, 126.9, 127.0, 127.1, 127.2, 127.5, 127.6, 128.3, 128.5, 128.6, 130.4, 140.0, 148.8, 154.1, 154.5, 154.9, 157.8, 161.5, 163.4; LCQ-MS ( $\text{M} + \text{H}^+$ ) calcd for  $\text{C}_{43}\text{H}_{58}\text{F}_3\text{N}_4\text{O}_7$  799.4252, found 799; LC-TOF ( $\text{M} + \text{H}^+$ ) calcd for  $\text{C}_{43}\text{H}_{58}\text{F}_3\text{N}_4\text{O}_7$  799.4252, found 799.4258.

**(9b).** **9b** was synthesized by general methods A and B using aldehyde **8a** as the starting material (58%):  $^1\text{H}$  NMR (500 MHz,  $\text{CDCl}_3$ )  $\delta$  1.35–1.55 (m, 27H), 2.20–2.40 (s, 3H), 2.50–2.80 (m, 2H), 2.80–2.95 (m, 1H), 3.00–3.21 (m, 2H), 3.30–3.79 (m, 6H), 3.80–4.00 (m, 2H), 5.10–5.25 (s, 2H), 6.60–6.70 (br s, 1H), 7.00–7.30 (m, 8H), 7.31–7.60 (m, 2H);  $^{13}\text{C}$  NMR (125 MHz,  $\text{CDCl}_3$ )  $\delta$  14.4, 21.2, 21.3, 27.8, 28.1, 28.4, 28.5, 28.7, 29.9, 34.8, 42.3, 42.9, 47.5, 47.7, 49.0, 49.4, 50.1, 50.4, 50.9, 60.6, 67.9, 76.9, 78.9, 79.3, 79.7, 79.8, 80.6, 81.4, 113.0, 113.1, 117.2, 117.5, 120.1, 121.4, 126.7, 126.8, 126.9, 127.0, 127.1, 127.2, 127.5, 127.6, 128.3, 128.5, 128.6, 130.4, 140.0, 148.8, 154.1, 154.5, 154.9, 157.8, 161.5, 163.4; LCQ-MS ( $\text{M} + \text{H}^+$ ) calcd for  $\text{C}_{43}\text{H}_{58}\text{F}_3\text{N}_4\text{O}_7$  799.4252, found 799; LC-TOF ( $\text{M} + \text{H}^+$ ) calcd for  $\text{C}_{43}\text{H}_{58}\text{F}_3\text{N}_4\text{O}_7$  799.4252, found 799.4248.

**(9c).** **9c** was synthesized by general methods A and B using aldehyde **8a** as the starting material (48%):  $^1\text{H}$  NMR (500 MHz,  $\text{CDCl}_3$ )  $\delta$  1.20–1.50 (m, 27H), 2.25–2.35 (m, 3H), 2.45–2.65 (m, 1H), 2.66–2.70 (m, 1H), 2.80–2.95 (m, 1H), 3.00–3.10 (m, 2H), 3.10–3.20 (m, 1H), 3.25–3.70 (m, 7H), 3.80–4.00 (m, 1H), 5.10–5.20 (m, 2H), 6.60–6.70 (m, 1H), 7.00–7.15 (m, 2H), 7.16–7.20 (m, 1H), 7.21–7.27 (m, 4H), 7.35–7.60 (m, 3H);  $^{13}\text{C}$  NMR (125 MHz,  $\text{CDCl}_3$ )  $\delta$  13.7, 14.2, 19.1, 21.0, 21.1, 24.7, 27.91, 27.96, 28.01, 28.2, 28.3, 28.5, 30.6, 34.4, 34.5, 34.6, 42.0, 42.1, 42.6, 42.7, 47.4, 47.5, 47.6, 47.8, 48.8, 49.3, 49.9, 50.1, 50.3, 50.8, 53.4, 53.8, 54.0, 60.4, 64.4, 67.7, 67.8, 68.0, 78.7, 78.8, 79.1, 79.2, 79.3, 79.6, 80.3, 81.17, 81.22, 115.2, 115.4, 115.6, 115.7, 117.0, 117.1, 119.9, 126.5, 126.6, 126.9, 127.0, 127.5, 128.1, 131.5, 139.7, 139.8, 148.6, 153.9, 154.3, 154.4, 154.5, 154.6, 154.7, 154.8, 155.1, 157.4, 157.5, 157.6, 162.7, 164.6, 171.2; LC-TOF ( $\text{M} + \text{H}^+$ ) calcd for  $\text{C}_{43}\text{H}_{58}\text{F}_3\text{N}_4\text{O}_7$  799.4258, found 799.4237.

**(9d).** **9d** was synthesized by general methods A and B using aldehyde **8a** as the starting material (55%):  $^1\text{H}$  NMR (500 MHz,  $\text{CDCl}_3$ )  $\delta$  1.20–1.50 (m, 27H), 2.25–2.35 (m, 3H), 2.45–2.65 (m, 1H), 2.66–2.71 (m, 1H), 2.80–2.95 (m, 1H), 3.00–3.10 (m, 1H), 3.10–3.20 (m, 1H), 3.25–3.70 (m, 7H), 3.80–4.00 (m, 2H), 5.10–5.20 (m, 2H), 6.60–6.70 (m, 1H), 7.00–7.60 (m, 12H);  $^{13}\text{C}$  NMR (125 MHz,  $\text{CDCl}_3$ )  $\delta$  13.7, 14.2, 19.1, 21.0, 21.1, 24.7, 27.91, 27.96, 28.01, 28.2, 28.3, 28.5, 30.6, 34.4, 34.5, 34.6, 42.0, 42.1, 42.6, 42.7, 47.4, 47.5, 47.6, 47.8, 48.8, 49.3, 49.9, 50.1, 50.3, 50.8, 53.4, 53.8, 54.0, 60.4, 64.4, 67.7, 67.8, 68.0, 78.7, 78.8, 79.1, 79.2, 79.3, 79.6, 80.3, 81.17, 81.22, 115.2, 115.4, 115.6, 115.7, 117.0, 117.1, 119.9, 126.5, 126.6, 126.9, 127.0, 127.5, 128.1, 131.5, 139.7, 139.8, 148.6, 153.9, 154.3, 154.4, 154.5, 154.6, 154.7, 154.8, 155.1, 157.4, 157.5, 157.6, 162.7, 164.6, 171.2; LC-TOF ( $\text{M} + \text{H}^+$ ) calcd for  $\text{C}_{43}\text{H}_{59}\text{F}_2\text{N}_4\text{O}_7$  781.4352, found 781.4366.

**(9f).** **9f** was synthesized by general methods A and B using aldehyde **8b** as the starting material (55%):  $^1\text{H}$  NMR (500 MHz,  $\text{CDCl}_3$ )  $\delta$  1.40–1.55 (m, 27H), 2.27–2.29 (m, 3H), 2.45–2.67 (m, 1H), 2.68–2.75 (m, 1H), 2.85–2.95 (m, 1H), 3.00–3.11 (m, 1H), 3.12–3.20 (m, 1H), 3.30–3.45 (m, 3H), 3.46–3.65 (m, 3H), 4.05–4.20 (m, 2H), 5.16 (s, 2H), 6.67 (s, 1H), 7.17–7.20 (m, 1H), 7.21–7.26 (m, 4H), 7.30–7.45 (m, 2H), 7.50–7.70 (m, 1H),

7.75–7.85 (m, 1H), 8.60–8.71 (m, 1H);  $^{13}\text{C}$  NMR (125 MHz,  $\text{CDCl}_3$ )  $\delta$  14.2, 21.11, 21.13, 24.7, 28.0, 28.1, 28.2, 28.3, 28.5, 29.7, 34.4, 34.5, 36.6, 42.2, 42.6, 42.7, 47.6, 47.7, 48.0, 48.8, 49.2, 49.89, 49.92, 50.1, 50.2, 50.8, 60.4, 67.5, 67.6, 67.7, 78.7, 79.1, 79.6, 80.2, 81.1, 81.2, 117.0, 117.1, 120.0, 120.4, 120.5, 124.76, 124.84, 126.4, 126.5, 126.6, 126.9, 127.0, 128.06, 128.11, 136.9, 137.0, 139.8, 139.9, 148.5, 149.3, 149.5, 153.8, 154.3, 154.4, 154.5, 154.7, 155.0, 155.4, 157.7; LC-TOF ( $\text{M} + \text{H}^+$ ) calcd for  $\text{C}_{42}\text{H}_{58}\text{F}_2\text{N}_5\text{O}_7$  782.4304, found 782.4299.

**(3a).** **3a** was synthesized by general methods C and D using **9a** as the starting material (95%):  $^1\text{H}$  NMR (500 MHz,  $\text{D}_2\text{O}$ )  $\delta$  2.29 (s, 3H), 2.78–2.81 (m, 2H), 2.95–3.05 (dd,  $J = 8.0, 15.0$  Hz, 1H), 3.15–3.20 (t,  $J = 6.0$ , 1H), 3.31–3.35 (dd,  $J = 3.0, 13.0$  Hz, 1H), 3.40–3.55 (m, 3H), 3.63–3.66 (d,  $J = 13.0$  Hz, 1H), 3.71–3.79 (m, 1H), 3.87–3.95 (m, 3H), 4.24–4.26 (t,  $J = 3.0$  Hz, 1H), 6.55 (s, 1H), 6.64 (s, 1H), 7.25–7.29 (dt,  $J = 2.5, 8.5$  Hz, 1H), 7.34–7.36 (dd,  $J = 2.5, 14.0$  Hz, 1H), 7.38–7.40 (dd,  $J = 2.5, 8.0$  Hz, 1H), 7.49–7.52 (dd,  $J = 6.0, 8.0$  Hz, 1H);  $^{13}\text{C}$  NMR (125 MHz,  $\text{D}_2\text{O}$ )  $\delta$  21.0, 29.1, 41.3, 47.0, 47.5, 49.2, 51.5, 51.7, 51.9, 63.6, 78.3, 110.4, 112.3, 112.5, 114.0, 118.2, 118.4, 118.6, 121.0, 131.2, 131.3, 134.2, 145.5, 153.9, 158.1, 161.4, 163.3; LC-TOF ( $\text{M} + \text{H}^+$ ) calcd for  $\text{C}_{21}\text{H}_{28}\text{F}_3\text{N}_4\text{O}$  409.2215, found 409.2226.

**(3b).** **3b** was synthesized by general methods C and D using **9b** as the starting material (100%):  $^1\text{H}$  NMR (500 MHz,  $\text{D}_2\text{O}$ )  $\delta$  2.29 (s, 3H), 2.78–2.81 (m, 2H), 2.95–3.05 (dd,  $J = 8.0, 15.0$  Hz, 1H), 3.15–3.20 (t,  $J = 6.0$ , 1H), 3.31–3.35 (dd,  $J = 3.0, 13.0$  Hz, 1H), 3.40–3.55 (m, 3H), 3.63–3.66 (d,  $J = 13.0$  Hz, 1H), 3.71–3.79 (m, 1H), 3.87–3.95 (m, 3H), 4.24–4.26 (t,  $J = 3.0$  Hz, 1H), 6.55 (s, 1H), 6.64 (s, 1H), 7.25–7.29 (dt,  $J = 2.5, 8.5$  Hz, 1H), 7.34–7.36 (dd,  $J = 2.5, 14.0$  Hz, 1H), 7.38–7.40 (dd,  $J = 2.5, 8.0$  Hz, 1H), 7.49–7.52 (dd,  $J = 6.0, 8.0$  Hz, 1H);  $^{13}\text{C}$  NMR (125 MHz,  $\text{D}_2\text{O}$ )  $\delta$  21.0, 29.1, 41.3, 47.0, 47.5, 49.2, 51.5, 51.7, 51.9, 63.6, 78.3, 110.4, 112.3, 112.5, 114.0, 118.2, 118.4, 118.6, 121.0, 131.2, 131.3, 134.2, 145.5, 153.9, 158.1, 161.4, 163.3; LC-TOF ( $\text{M} + \text{H}^+$ ) calcd for  $\text{C}_{21}\text{H}_{28}\text{F}_3\text{N}_4\text{O}$  409.2215, found 409.2223.

**(3c).** **3c** was synthesized by general methods C and D using **9c** as the starting material (95%):  $^1\text{H}$  NMR (500 MHz,  $\text{D}_2\text{O}$ )  $\delta$  2.30 (s, 3H), 2.78–2.81 (m, 2H), 2.95–3.05 (dd,  $J = 8.0, 15.0$  Hz, 1H), 3.15–3.20 (t,  $J = 6.0$ , 1H), 3.31–3.35 (dd,  $J = 3.0, 13.0$  Hz, 1H), 3.40–3.55 (m, 3H), 3.63–3.66 (d,  $J = 13.0$  Hz, 1H), 3.71–3.79 (m, 1H), 3.87–3.95 (m, 3H), 4.24–4.26 (t,  $J = 3.0$  Hz, 1H), 6.55 (s, 1H), 6.64 (s, 1H), 7.21–7.25 (dd,  $J = 8.5, 8.5$  Hz, 2H), 7.59–7.62 (dd,  $J = 5.0, 8.5$  Hz, 2H);  $^{13}\text{C}$  NMR (125 MHz,  $\text{D}_2\text{O}$ )  $\delta$  21.0, 29.0, 41.3, 47.0, 47.4, 49.2, 51.7, 51.9, 51.9, 63.6, 78.3, 110.4, 113.9, 116.0, 116.1, 118.7, 127.42, 127.47, 127.55, 127.59, 145.5, 153.9, 158.1; LC-TOF ( $\text{M} + \text{H}^+$ ) calcd for  $\text{C}_{21}\text{H}_{28}\text{F}_3\text{N}_4\text{O}$  409.2215, found 409.2230.

**(3d).** **3d** was synthesized by general methods C and D using **9d** as the starting material (95%):  $^1\text{H}$  NMR (500 MHz,  $\text{D}_2\text{O}$ )  $\delta$  2.30 (s, 3H), 2.73–2.84 (m, 2H), 2.95–3.05 (dd,  $J = 8.5, 15.0$  Hz, 1H), 3.10–3.20 (t,  $J = 6.0$ , 1H), 3.31–3.35 (dd,  $J = 3.0, 13.5$  Hz, 1H), 3.40–3.55 (m, 3H), 3.63–3.66 (d,  $J = 13.5$  Hz, 1H), 3.71–3.79 (m, 1H), 3.87–3.95 (m, 3H), 4.24–4.26 (t,  $J = 3.0$  Hz, 1H), 6.55 (s, 1H), 6.64 (s, 1H), 7.45–7.65 (m, 5H);  $^{13}\text{C}$  NMR (125 MHz,  $\text{D}_2\text{O}$ )  $\delta$  21.0, 29.0, 41.3, 47.0, 47.4, 49.2, 51.6, 51.8, 52.0, 63.6, 78.2, 110.4, 113.9, 119.0, 120.9, 124.81, 124.86, 124.91, 129.1, 131.6, 131.9, 132.1, 145.5, 153.9, 158.1; LC-TOF ( $\text{M} + \text{H}^+$ ) calcd for  $\text{C}_{21}\text{H}_{29}\text{F}_2\text{N}_4\text{O}$  391.2309, found 391.2337.

**(3e).** **3e** was synthesized by general methods C and D using **9e** as the starting material (96%):  $^1\text{H}$  NMR (500 MHz,  $\text{D}_2\text{O}$ )  $\delta$  0.85–0.95 (d,  $J = 2.5, 3\text{H}$ ), 1.45–1.55 (m, 1H), 1.61–1.70 (m, 1H), 1.71–1.97 (m, 3H), 2.00–2.10 (m, 1H), 2.35–2.45 (m, 1H), 2.46–2.57 (m, 1H), 2.90–3.00 (t,  $J = 6.0$ , 1H), 3.16–3.21 (m, 1H), 3.30–3.50 (m, 4H), 3.51–3.60 (d,  $J = 13.5$  Hz, 1H), 3.61–3.70 (m, 1H), 3.75–3.90 (m, 3H), 4.14s–4.16 (t,  $J = 3.0$  Hz, 1H), 7.45–7.65 (m, 5H);  $^{13}\text{C}$  NMR (125 MHz,  $\text{D}_2\text{O}$ )  $\delta$  17.5, 17.6, 18.2, 26.8, 27.2, 27.3, 32.6, 32.9, 40.0, 40.2, 48.3, 48.9, 49.1, 49.6, 50.6, 52.2, 58.8, 65.2, 79.9, 80.0, 115.4, 115.6, 116.8, 117.0,



**Table 3.** Crystallographic Data Collection and Refinement Statistics

data set <sup>a</sup>	nNOS-3a	nNOS-3b	nNOS-3c	nNOS-3d
<b>Data collection</b>				
PDB code	3NLV	3NLX	3NLY	3NLZ
Space group	<i>P2<sub>1</sub>2<sub>1</sub>2<sub>1</sub></i>	<i>P2<sub>1</sub>2<sub>1</sub>2<sub>1</sub></i>	<i>P2<sub>1</sub>2<sub>1</sub>2<sub>1</sub></i>	<i>P2<sub>1</sub>2<sub>1</sub>2<sub>1</sub></i>
Cell dimensions				
<i>a</i> , <i>b</i> , <i>c</i> (Å)	52.3, 111.7, 164.4	52.3, 111.5, 164.4	51.8, 111.2, 164.1	51.9, 110.4, 164.0
Resolution (Å)	2.10 (2.14–2.10)	1.87 (1.90–1.87)	2.00 (2.03–2.00)	1.92 (1.95–1.92)
<i>R</i> <sub>sym</sub> or <i>R</i> <sub>merge</sub>	0.080 (0.59)	0.053 (0.36)	0.078 (0.40)	0.050 (0.32)
<i>I</i> / <i>σI</i>	9.1 (2.2)	13.5 (3.9)	7.6 (1.8)	11.5 (2.6)
No. unique reflections	56857	79054	63439	73017
Completeness (%)	99.4 (99.5)	98.2 (96.5)	96.7 (80.9)	99.4 (89.8)
Redundancy	5.6 (2.9)	4.1 (4.1)	3.9 (3.1)	4.1 (3.6)
<b>Refinement</b>				
Resolution (Å)	2.10	1.87	2.00	1.92
No. reflections used	54011	75069	60245	69320
<i>R</i> <sub>work</sub> / <i>R</i> <sub>free</sub>	0.175/0.211	0.178/0.209	0.201/0.249	0.173/0.210
No. atoms				
Protein	6671	6689	6676	6707
Ligand/ion	187	223	190	217
Water	434	479	190	417
Rms deviations				
Bond lengths (Å)	0.013	0.012	0.015	0.013
Bond angles (deg)	1.325	1.390	1.554	1.456
<hr/>				
data set <sup>a</sup>	nNOS-3e	nNOS-3f	eNOS-3b	eNOS-3f
<b>Data collection</b>				
PDB code	3NM0	3NLW	3NLU	3NLT
Space group	<i>P2<sub>1</sub>2<sub>1</sub>2<sub>1</sub></i>	<i>P2<sub>1</sub>2<sub>1</sub>2<sub>1</sub></i>	<i>P2<sub>1</sub>2<sub>1</sub>2<sub>1</sub></i>	<i>P2<sub>1</sub>2<sub>1</sub>2<sub>1</sub></i>
Cell dimensions				
<i>a</i> , <i>b</i> , <i>c</i> (Å)	52.1, 110.9, 164.2	52.2, 111.4, 164.7	58.0, 107.0, 156.9	57.9, 106.9, 157.0
Resolution (Å)	1.81 (1.84–1.81)	2.10 (2.14–2.10)	2.65 (2.70–2.65)	2.75 (2.80–2.75)
<i>R</i> <sub>sym</sub> or <i>R</i> <sub>merge</sub>	0.048 (0.38)	0.069 (0.55)	0.121(0.58)	0.103 (0.65)
<i>I</i> / <i>σI</i>	12.1 (2.7)	9.2 (2.4)	9.7 (1.9)	12.4 (1.9)
No. unique reflections	86908	56364	28366	25670
Completeness (%)	99.0 (92.5)	99.2 (100.0)	97.3 (99.1)	95.6 (94.4)
Redundancy	4.0 (3.8)	4.1 (4.1)	3.7 (3.7)	3.9 (4.0)
<b>Refinement</b>				
Resolution (Å)	1.81	2.10	2.65	2.74
No. reflections used	82532	53523	26957	24379
<i>R</i> <sub>work</sub> / <i>R</i> <sub>free</sub> <sup>b</sup>	0.178/0.209	0.171/0.207	0.185/0.254	0.186/0.262
No. atoms				
Protein	6716	6676	6451	6419
Ligand/ion	217	185	197	195
Water	459	319	111	60
Rms deviations				
Bond lengths (Å)	0.013	0.013	0.014	0.014
Bond angles (deg)	1.360	1.347	1.502	1.519

<sup>a</sup> See Schemes 2–4 for nomenclature and chemical formula of inhibitors. <sup>b</sup> *R*<sub>free</sub> was calculated with the 5% of reflections set aside throughout the refinement. For each NOS isoform, the set of reflections for the *R*<sub>free</sub> calculation were kept the same for all data sets according to those used in the data of the starting model.

126.0, 132.1, 132.2, 140.2, 163.1, 165.0, 168.4; LC-TOF (M + H<sup>+</sup>) calcd for C<sub>21</sub>H<sub>33</sub>F<sub>2</sub>N<sub>4</sub>O 395.2622, found 395.2633.

(3f). **3f** was synthesized by general methods C and D using **9f** as the starting material (100%): <sup>1</sup>H NMR (500 MHz, D<sub>2</sub>O) δ 1.40–1.50 (m, 1H), 1.51–1.60 (m, 2H), 1.79–1.90 (m, 2H), 1.91–1.98 (d, *J* = 13.5 Hz, 1H), 2.20 (s, 3H), 2.65–2.75 (m, 1H), 2.79–2.85 (m, 1H), 2.94–2.96 (d, *J* = 7.5 Hz, 1H), 2.97–3.00 (m, 1H), 3.07–3.12 (dd, *J* = 11.5, 11.5 Hz, 1H), 3.20–3.26 (dd, *J* = 0.5, 13.0 Hz, 1H), 3.31–3.47 (m, 4H), 3.52–3.55 (d, *J* = 13.5 Hz, 1H), 3.61–3.64 (m, 1H), 3.74–3.82 (m, 5H), 4.11 (s, 1H), 6.52 (s, 1H), 6.57 (s, 1H); <sup>13</sup>C NMR (125 MHz, D<sub>2</sub>O) δ 20.4, 21.05, 21.06, 22.4, 28.95, 29.01, 41.48, 41.51, 45.1, 47.0, 48.08, 48.14, 49.4, 57.7, 63.7, 63.9, 78.3, 78.4, 110.4, 114.09, 114.12, 145.7, 153.9, 158.1; LC-TOF (M + H<sup>+</sup>) calcd for C<sub>20</sub>H<sub>34</sub>F<sub>2</sub>N<sub>5</sub>O 398.2742, found 398.2726.

**3. Enzyme Assays.** The three isozymes, murine macrophage iNOS, rat nNOS, and bovine eNOS, were recombinant enzymes,

overexpressed (in *Escherichia coli*) and isolated as reported.<sup>27</sup> IC<sub>50</sub> values for inhibitors **3a–f** were measured for the three different isoforms of NOS using L-arginine as a substrate. The formation of nitric oxide was measured using a hemoglobin capture assay described previously.<sup>24</sup> All NOS isozymes were assayed at room temperature in a 100 mM Hepes buffer (pH 7.4) containing 10 μM L-arginine, 1.6 mM CaCl<sub>2</sub>, 11.6 μg/mL calmodulin, 100 μM DTT, 100 μM NADPH, 6.5 μM H<sub>4</sub>B, 3.0 μM oxyhemoglobin (for iNOS assays, no Ca<sup>2+</sup> and calmodulin were added). The assay was initiated by the addition of enzyme, and the initial rates of the enzymatic reactions were determined by monitoring the formation of NO–hemoglobin complex at 401 nm for 60 s. The corresponding

(27) (a) Hevel, J. M.; White, K. A.; Marletta, M. *J. Biol. Chem.* **1991**, *266* (34), 22789. (b) Roman, L. J.; Sheta, E. A.; Martásek, P.; Gross, S. S.; Liu, Q.; Masters, B. S. S. *Proc. Natl. Acad. Sci. U.S.A.* **1995**, *92* (18), 8428. (c) Martásek, P.; Liu, Q.; Roman, L. J.; Gross, S. S.; Sessa, W. C.; Masters, B. S. S. *Biochem. Biophys. Res. Commun.* **1996**, *219* (2), 359.

$K_i$  values of inhibitors were calculated from the  $IC_{50}$  values using eq 1 with known  $K_m$  values (rat nNOS, 1.3  $\mu$ M; iNOS, 8.3  $\mu$ M; eNOS, 1.7  $\mu$ M).

$$K_i = IC_{50}/(1 + [S]/K_m) \quad (1)$$

**4. Inhibitor Complex Crystal Preparation.** The nNOS or eNOS heme domain proteins used for crystallographic studies were produced by limited trypsin digest from the corresponding full-length enzymes and further purified through a Superdex 200 gel filtration column (GE Healthcare) as described previously.<sup>28</sup> The enzyme–inhibitor complex crystals were obtained by soaking rather than co-crystallization as reported in the earlier structural work.<sup>29</sup> The nNOS heme domain at 7–9 mg/mL containing 20 mM histidine or the eNOS heme domain at 20 mg/mL with 2 mM imidazole was used for the sitting drop vapor diffusion crystallization setup under the conditions reported before.<sup>28,30</sup> Fresh crystals (1–2 day old) were first passed stepwise through cryo-protectant solutions described<sup>28,30</sup> and then soaked with 10 mM inhibitor for 4–6 h at 4 °C before being mounted on nylon loops and flash cooled by plunging into liquid nitrogen. Crystals were stored in liquid nitrogen until data collection.

**5. X-ray Diffraction Data Collection, Processing, and Structure Refinement.** The cryogenic (100 K) X-ray diffraction data were collected remotely at various beamlines at Stanford Synchrotron Radiation Lightsource through the data collection control software Blu-Ice<sup>31</sup> and the crystal mounting robot. Raw data frames were indexed, integrated, and scaled using HKL2000.<sup>32</sup> Typically, each data set consisted of 90–100° of data with a 0.5° frame width for both nNOS and eNOS crystals because of their identical orthorhombic  $P2_12_12_1$  space group symmetry.

The binding of inhibitors was detected by the initial difference Fourier maps calculated with REFMAC.<sup>33</sup> The inhibitor molecules

were then modeled in O<sup>34</sup> or COOT<sup>35</sup> and refined using REFMAC. Water molecules were added in REFMAC and checked by COOT. The TLS<sup>36</sup> protocol was implemented in the final stage of refinements with each subunit as one TLS group. The refined structures were validated in COOT before deposition to RCSB protein data bank. The crystallographic data collection and structure refinement statistics are summarized in Table 3 with PDB accession codes included.

**6. Molecular Mechanics Poisson–Boltzmann/SurfaceA (MM-PBSA) Method for Free Energy of Binding of Inhibitors.** The MM-PBSA method<sup>26</sup> as implemented in Amber 9.0 was used to compute the free energy of binding of inhibitors to NOS and was previously described in detail.<sup>23</sup> To briefly summarize, the free energies of 10 different aminopyridine inhibitors–NOS complexes were calculated from a single energy minimized structure starting from the known crystal structures described in our previous work.<sup>23</sup> A plot of the resulting computed free energy (PB) versus  $\Delta G_{\text{exp}}$  was obtained from experimental  $K_i$  values. The empirical equation derived from Figure 5,  $\Delta G_{\text{calc}} = (\text{PB} - 5.2874)/6.029$ , was used to calculate free energies of binding for the inhibitors used in the present study.

**7. Pharmacokinetic Data.** All pharmacokinetic results were obtained by LC–MS–MS analysis and calculation of PK parameters using WinNonlin software at BioDuro, Inc., Shanghai, China.

**Acknowledgment.** The authors are grateful for financial support from the National Institutes of Health (GM49725 to R.B.S. and GM57353 to T.L.P.). We thank Dr. Bettie Sue Siler Masters (NIH grant GM52419, with whose laboratory P.M. and L.J.R. are affiliated). B.S.S.M. also is grateful to the Welch Foundation for a Robert A. Welch Distinguished Professorship in Chemistry (AQ0012). P.M. is supported by grants 0021620806 and 1M0520 from MSMT of the Czech Republic. We also thank the staff at SSRL for their assistance during the remote X-ray diffraction data collections.

**Supporting Information Available:** Copies of complete spectroscopic data of compounds **9a–d**, **9f**, and **3a–f**. This material is available free of charge via the Internet at <http://pubs.acs.org>.

JA106175Q

- (28) Li, H.; Shimizu, H.; Flinspach, M.; Jamal, J.; Yang, W.; Xian, M.; Cai, T.; Wen, E. Z.; Jia, Q.; Wang, P. G.; Poulos, T. L. *Biochemistry* **2002**, *41*, 13868.
- (29) Flinspach, M. L.; Li, H.; Jamal, J.; Yang, W.; Huang, H.; Hah, J. M.; Gomez-Vidal, J. A.; Litzinger, E. A.; Silverman, R. B.; Poulos, T. L. *Nat. Struct. Mol. Biol.* **2004**, *11*, 54.
- (30) Raman, C. S.; Li, H.; Martasek, P.; Kral, V.; Masters, B. S.; Poulos, T. L. *Cell* **1998**, *95*, 939.
- (31) McPhillips, T. M.; McPhillips, S. E.; Chiu, H. J.; Cohen, A. E.; Deacon, A. M.; Ellis, P. J.; Garman, E.; Gonzalez, A.; Sauter, N. K.; Phizackerley, R. P.; Soltis, S. M.; Kuhn, P. J. *Synchrotron Radiat.* **2002**, *9*, 401.
- (32) Otwinowski, Z.; Minor, W. *Methods Enzymol.* **1997**, *276*, 307.
- (33) Murshudov, G. N.; Vagin, A. A.; Dodson, E. J. *Acta Crystallogr.* **1997**, *D53*, 240.

- (34) Jones, T. A.; Zou, J.-Y.; Cowan, S. W.; Kjeldgaard, M. *Acta Crystallogr.* **1991**, *A47*, 110.

- (35) Emsley, P.; Cowtan, K. *Acta Crystallogr.* **2004**, *D60*, 2126.

- (36) Winn, M. D.; Isupov, M. N.; Murshudov, G. N. *Acta Crystallogr.* **2001**, *D57*, 122.